*Article*

# A Simulation Independent Analysis of Single- and Multi-Component cw ESR Spectra

**Aritro Sinha Roy [1] 0000-0001-5900-1997, Boris Dzikovski[2], Dependu Dolui [3] 0000-0003-3296-7489, Olga Makhlynets[4], Arnab Dutta[5] 0000-0002-9998-6329, and Madhur Srivastava [1,6]* 0000-0002-2095-0412**

1 Department of Chemistry and Chemical Biology, Cornell University; as836@cornell.edu
2 National Biomedical Center for Advanced ESR Technology, Cornell University; bd55@cornell.edu
3 Department of Chemistry, Indian Institute of Technology Bombay; dolui.iitb@gmail.com
4 Department of Chemistry, Syracuse University; ovmakhly@syr.edu
5 Department of Chemistry, Indian Institute of Technology Bombay; arnabdutta@chem.iitb.ac.in
6 National Biomedical Center for Advanced ESR Technology, Cornell University; ms2736@cornell.edu
* Correspondence: ms2736@cornell.edu

**Abstract:** Accurate analysis of continuous-wave electron spin resonance (cw ESR) spectra of biological or organic free-radicals and paramagnetic metal complexes is key to understand their structure-function relationships and electrochemical properties. Current method of analysis based on simulations often fail to extract the spectral information accurately. In addition, such analyses are highly sensitive to spectral resolution and artifacts, users' defined input parameters and spectral complexity. We introduce a simulation-independent spectral analysis approach that enables broader application of ESR. We use a wavelet packet transform-based method for extracting g values and hyperfine (A) constants directly from cw ESR spectra. We show that our method overcomes the challenges associated with simulation-based methods for analyzing poorly / partially resolved and unresolved spectra, which is a common in most cases. The accuracy and consistency of the method are demonstrated on a series of experimental spectra of organic radicals and copper-nitrogen complexes. We showed that for a two-component system, the method identifies their individual spectral features even at a relative concentration of 5% for the minor component.

**Keywords:** ESR spectral analysis; hyperfine decoupling; resolution enhancement; wavelet packet transform; simulation-free spectra analysis

## 1. Introduction

ESR spectroscopy is a useful and powerful tool for studying biological free radicals and transition metal cofactors in proteins [1–7]. Understanding the electronic structure and local environment in such systems provides important insights in catalytic mechanisms [8–13] and redox processes in biological systems [6,14–16]. However, extracting information from ESR spectra can be challenging, especially in the case of weak and poorly resolved coupling interactions between studied spins. Traditionally, ESR spectral analysis is carried out by the spectral simulations, followed by user interpretation, which not only introduce bias, but impairs the consistency of such analysis. The low-intensity signal components are difficult to analyze through standard spectral simulations in a variety of cases [17–19]. Accurate spectral analysis in such cases require quantum chemical computations or special techniques [20–22], but without sufficient expertise and knowledge in the field, the interpretations rely heavily on the researchers' experience and intuition than the robustness of the method. An even more challenging problem, which occurs frequently, is the presence of more than one structurally similar molecules in a system. For closely resembling species, identifying multiple components by ESR alone could be a daunting task and the standard simulation tools are incapable of extracting such information from the spectra without user manipulation. Additionally, every standard ESR simulation methods requires user defined starting configuration for optimization [23,24], which could lead to overfitting and/or unintended manipulation. Hence, direct extraction of the relevant spin hamiltonian parameters, namely the $g$-factors and and hyperfine coupling constant ($A$) values from

 doi:10.20944/preprints202303.0377.v1



an experimental ESR spectrum would be ideal. The extracted parameter values can be used directly to interpret the electronic structure or if needed, can be further optimized by standard spectral fitting software.

The capability of the wavelet transform in picking periodic hyperfine pattern from poorly resolved ESR spectra was highlighted previously [25]. In a series of recent publications [26–28], we have presented an improved version of the wavelet transform based spectral analysis, which can decouple different frequency components in an ESR or nuclear magnetic resonance (NMR) spectrum, enhancing the resolution and providing an opportunity to extract spectral information or parameters in a selective and objective manner. We have modified the Noise Elimination and Reduction via Denoising (NERD) method [25,29], which is based on the discrete wavelet transform (DWT) method, for separation of the hyperfine lines in cw ESR spectra and extraction of spectral parameters initially [26]. Later, in analyzing $^{1}$H NMR spectra of molecular mixtures, which features highly overlapped resonance lines due to the presence of scalar coupling between intramolecular protons, we recognized that spectral decomposition by the wavelet packet transform (WPT) is superior to DWT in separating the central frequencies from the multiplet structures encompassing them [27,28]. Using the same concept, a cw ESR spectrum is decomposed into its different frequency components by WPT and at an optimum level of decomposition, a detail component in the wavelet domain is used in extracting the hyperfine and/or superhyperfine structure, if any. The process has been explained with an illustrative example later in this work (cf. Method). In case of copper complexes, the analysis of the nitrogen-hyperfine structure is used in determination of both $g_{\perp}$ and hyperfine splitting by copper, $A_{\perp}(Cu)$.

The outcome of the method has been validated by comparing the extracted hyperfine coupling constant values from both partially resolved and unresolved ESR spectra of Tempol and Tempo, recorded in absence and in presence of oxygen, respectively. We demonstrate the consistency of the WPT based spectral analysis by using different wavelets in our analysis, namely Daubechies (Db6 and Db9) and Coiflet (coif3) wavelets. The method is applied across a wide range of copper complexes and both the copper- and nitrogen-hyperfine coupling constants are recovered from partially resolved and unresolved ESR spectra. The analysis didn't use any prior knowledge about the structure of the complexes or user defined inputs in deriving the spectral parameters. The derived coordination geometry aligned with the structure predicted from analog studies, independent experiments and/or quantum computation, which further validates the results obtained by the WPT-based spectral analysis. The $g$- and $A$-values obtained were compared with the optimized parameters obtained from spectral fitting by EasySpin software for a set of selected cases. The comparison shows that our method remains unaffected by artifacts, such as saturation and the passage effect, which affects simulations or spectral fitting significantly. While the performance of both the methods were at par for well resolved spectra, unresolved spectral feature remained inaccessible to the spectral fitting strategy. In those later cases, to the best of our knowledge, the proposed WPT-based analysis is the only method that can separate the so-called hidden features from poorly resolved spectra and extract the relevant spectral parameters by a direct analysis of an ESR spectrum. In this work, along with describing the extraction of spectral parameters by WPT analysis of the ESR spectra of nitroxides and copper complexes, we demonstrated the efficiency of the method in identifying and analysing multi-component spectra.

## 2. Method

### *2.1. Overview of the Wavelet Packet Transform Theory*

A continuous wavelet transform can be defined as [30],

$$F(\tau, s) = \frac{1}{\sqrt{|s|}} \int_{-\infty}^{+\infty} f(\delta)\psi^{*}\left(\frac{\delta - \tau}{s}\right) dt \quad (1)$$

where $s$ is the inverse frequency (or frequency range) parameter, $\tau$ is the signal localization parameter, $\delta$ represents the chemical shift, $f(\delta)$ is the spectrum, $F(\tau, s)$ is the wavelet-

Preprints (www.preprints.org) | NOT PEER-REVIEWED | Posted: 21 March 2023 doi:10.20944/preprints202303.0377.v1



transformed signal at a given signal localization and frequency and $\psi^*\left(\frac{\delta-\tau}{s}\right)$ is the signal probing function called "wavelet." Different wavelets are used to vary selectivity or sensitivity of adjacent frequencies with respect to signal localization. They are not dependent on *a priori* information of the signal or its characteristics.

Discrete wavelet transform (DWT) is expressed by two sets of wavelet components (Detail and Approximation) in the following way[30]:

$$D_j[n] = \sum_{m=0}^{p-1} f[\delta_m] 2^{\frac{j}{2}} \psi[2^j \delta_m - n] \tag{2}$$

$$A_j[n] = \sum_{m=0}^{p-1} f[\delta_m] 2^{\frac{j}{2}} \phi[2^j \delta_m - n] \tag{3}$$

where $f[\delta_m]$ is the discrete input spectrum, $p$ is the length of input signal $f[\delta_m]$, $D_j[n]$ and $A_j[n]$ are the Detail and Approximation components, respectively, at the $j^{th}$ decomposition level, and $\psi[2^j \delta_m - n]$ and $\phi[2^j \delta_m - n]$ are wavelet and scaling functions, respectively. The maximum number of decomposition levels that can be obtained is $N$, where $N = \log_2 p$, and $1 \leq j \leq N$. The scaling and wavelet functions, at a decomposition level, are orthogonal to each other, as they represent non-overlapping frequency information. Similarly, wavelet functions at different decomposition levels are orthogonal to each other.

The Detail component $D_j[n]$ is the discrete form of Equation 1, where $j$ and $n$ are associated with $s$ and $\tau$, respectively. The Approximation component $A_j[n]$ represent the remaining frequency bands not covered by the Detail components till $j^{\text{th}}$ level. The signal $f[\delta_m]$ can be reconstructed using the inverse discrete wavelet transform as follows,

$$f[\delta_m] = \sum_{k=0}^{p-1} A_{j_0}[k] \phi_{j_0,k}[\delta_m] + \sum_{j=1}^{j_0} \sum_{k=0}^{p-1} D_j[k] \psi_{j,k}[\delta_m] \tag{4}$$

where $j_0$ is the maximum decomposition level from which input signal needs to be reconstructed. Compared to that, both the Approximation and Detail components at each level are further decomposed into a set of Approximation and Detail components. A schematic diagram of DWT and WPT decomposition against increasing levels are shown for comparison in Figure 1 [27].

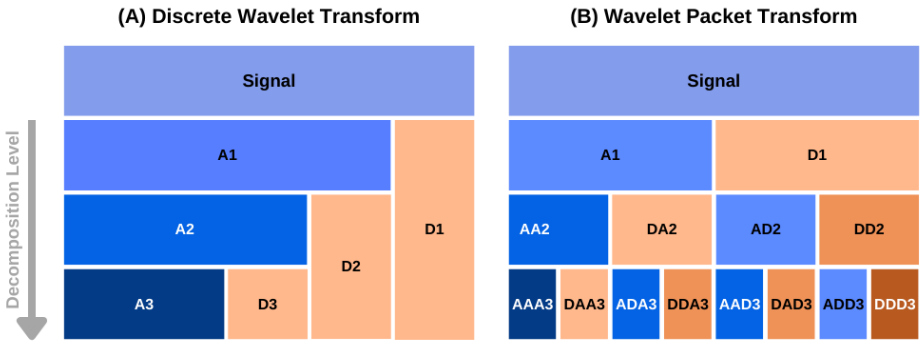


**Figure 1.** A schematic diagram of data decomposition in discrete (A) and packet wavelet transform (B) methods. The Approximation and Detain components at level $k$ is denoted as $A_k$ and $D_k$ in (A). In case of wavelet packet transform, the Approximation and Detail component at a decomposition level are denoted by the component name of the previous level followed by $A_k$ or $D_k$, respectively [27].

### *2.2. A Case Study: WPT Analysis of cw ESR Spectrum of Tempo*

In this section we explain the details of WPT spectral analysis by using the cw ESR spectrum of Tempo as an example, shown in Figure 2. The ESR spectrum of Tempo is

 doi:10.20944/preprints202303.0377.v1



split into three major lines, corresponding to the hyperfine coupling of the $^{14}N$ nucleus. Each of those lines are further split by the interaction of the $^{1}H$ nuclei in the molecule, giving rise to what we designate as the superhyperfine splitting. Our goal is to separate the superhyperfine or the fine structure of the Tempo spectrum from the rest. The first level of wavelet decomposition by the DB9 wavelet in the Figure 2 shows a pair of approximate (A1) and detail (D1) components. It can be seen that D1 comprises of noise and the entire spectrum is represented by A1. Hence, D1 and all the components that derive from D1 during successive decomposition are not used in the spectral analysis. Decomposition of A1 is continued till level-4, where the approximation component of AAA3 shows no superhyperfine splitting and correspondingly, the approximation component derived from the decomposition of DAA3 contains the superhyperfine splitting pattern. This is why, in this case, decomposition till level-4 is considered to be optimal in separating the hyperfine and superfine splittings of Tempo's ESR spectrum. For cases, where the superhyperfine is not resolved or visible, the optimum level of decomposition is chosen to be 4 based on previous work [26].

Preprints (www.preprints.org) | NOT PEER-REVIEWED | Posted: 21 March 2023 doi:10.20944/preprints202303.0377.v1



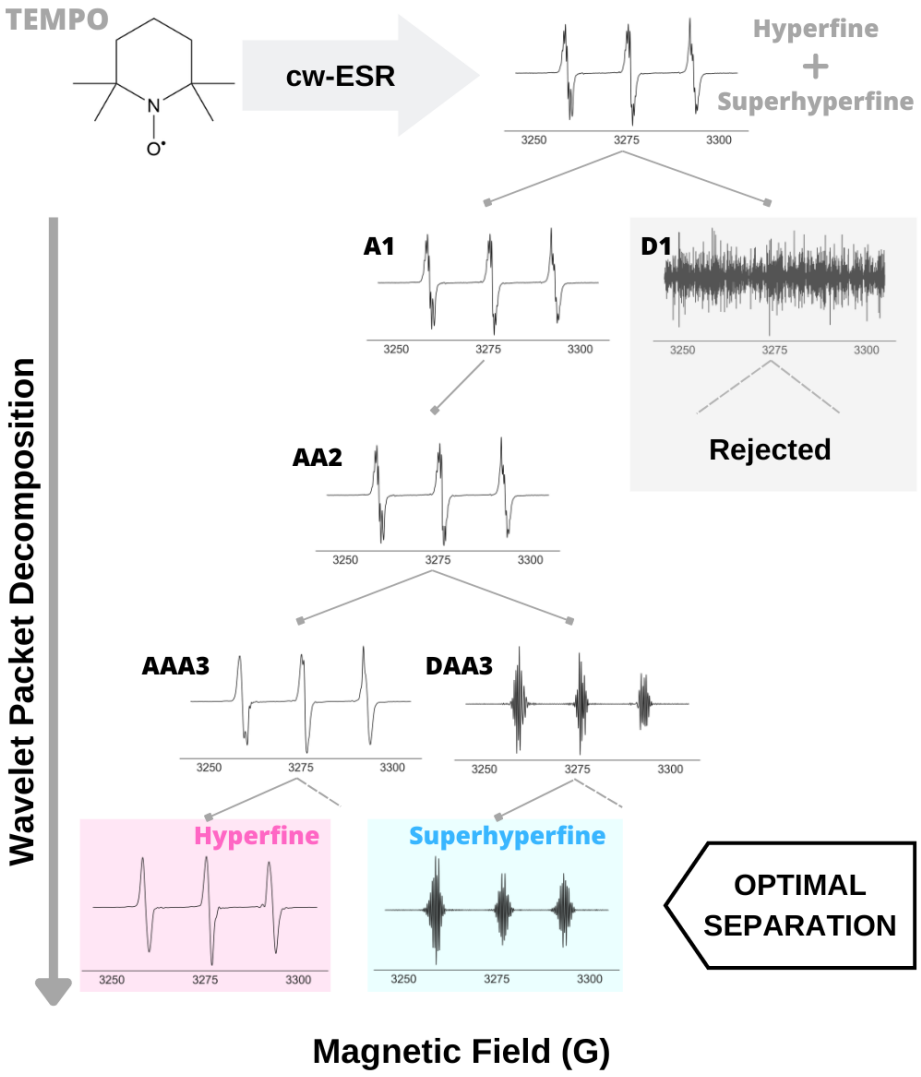


**Figure 2.** Separation of hyperfine and superhyperfine components in Tempo's ESR spectrum by WPT decomposition using Db9 wavelet. Given that at level-1, A1 contains all the spectral information, D1 and all the components derived from D1 are rejected. Complete separation of superhyperfine structure from the approximate component occurred after the decomposition level-3. Pure hyperfine and superfine components are produced in the approximation component of the decomposition of AAA3 and DAA3.

### 3. Materials

A series of experimental X-band ESR spectra were used in our analysis and the corresponding molecular structures are given in Table 1. ESR spectra of Tempol and Tempo are very well studied and we presented their spectral analysis by WPT for validation purpose. Mutation of superoxide dismutase-1 (SOD1) is arguably correlated with the incidence of significant fractions of familial, and spontaneous cases of amyotrophic lateral schlerosis (ALS) disease [31,32]. For one of its mutants, SOD1:H48Q, cw ESR spectrum was collected at 9.26 GHz, at a temperature of 30 K and concentration in the range of 300 to 350 $\mu$M using 50 $\mu$L 0.4 mm glass capillaries. No cryoprotectant was added given the viscous nature of the sample. Due to the presence of a glutamine residue in place of a histidine in the mutant, the nitrogen-hyperfine structure along the $g_{||}$ becomes partially resolved as a result of the reduction of the number of nitrogen in the copper coordination sphere. Cu-AHAHARA spectra were collected at 9.39 GHz for two different temperatures, 10 K

Preprints (www.preprints.org) | NOT PEER-REVIEWED | Posted: 21 March 2023 doi:10.20944/preprints202303.0377.v1



and 100 K. ESR measurements of CuQu and CuQuA were done in DMSO solutions at 100 K with an ESR frequency of 9.32 GHz.

**Table 1.** Molecular structures and ESR frequencies corresponding to the experimental cw ESR spectra used in this work.

| Molecule | Structure | ESR Frequency (GHz) |
|---|---|---|
| Tempo | 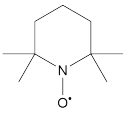 | 9.33 |
| Tempol | 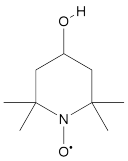 | 9.33 |
| SOD1:H48Q | SOD1 mutant, histidine (48) replaced with glutamine | 9.26 |
| Cu-AHAHARA | A complex of Cu (II) and AHAHARA peptide: C-terminus as amide and N-terminus as acetyl group | 9.39 |
| CuQu | 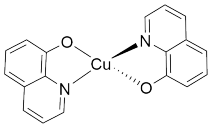 | 9.316 |
| CuQuA | 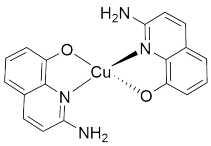 | 9.316 |

*3.1. Experimental Section*

3.1.1. Synthesis

**Copper quinoline (CuQuA):** 160.0 mg (1.0 mM) 2-amino-8-quinolinol was taken in an 80.0 mL Schlenk flask with a magnetic stirrer bar and 15.0 mL methanol was added to make it a homogeneous yellow colour solution. 85.0 mg (0.49 mM) $CuCl_2.2H_2O$ was taken separately with 10 mL MeOH in another Schlenk flask under the steam of $N_2$. Then, the two methanolic solutions were charged under nitrogen flow. An immediate dark brown solution appeared after adding the metal salt to the ligand. Reducing the solvent with continuous $N_2$/Ar flashing whitish deep brownish precipitate was observed. The reaction mixture was further stirred for two hours for completion with $N_2$ purging. Then the precipitate was collected, washed with hexane and diethyl ether and dried under a high vacuum (yield= 137.0 mg, 76% w.r.t. 2-amino-8-quinolinol). XRD-suitable crystals (CCDC 2127156) were grown from slow diffusion from methanol/diethyl ether solution.

 doi:10.20944/preprints202303.0377.v1



**Copper quinone (CuQu):** Synthesized as reported above, where 8-hydroxyquinoline was utilized as the precursor ligand (yield= 120.0 mg).

**Copper AHAHARA:** The AHAHARA peptide was synthesized by manual Fmoc solid-phase synthesis at elevated temperature using Amide Rink resin, Fmoc-protected amino acids and previously reported protocols [33].

**SOD1:H48Q:** The recombinant SOD1:H48Q protein, replacing a histidine with glutamine, was expressed and purified as described in a previous work [34].

### *3.2. ESR Experiments*

Oxygen-free samples of Tempol and Tempo were prepared by flame-sealing after a triple repeat of the freeze-thaw cycle under vacuum. Oxygen saturated samples were prepared by passing oxygen gas through the radical solution in water for 10 minutes and kept under oxygen atmosphere during measurements. Samples with an intermediate oxygen concentration were prepared and handled in air. The nitroxide concentration in all the samples was 100 $\mu$M. The ESR spectra were recorded at 293K at a microwave (MW) frequency of 9.33 GHz, power of 0.1 mW, modulation frequency of 100 kHz and modulation amplitude of 0.1 G. The ESR spectrum of SOD1:H48Q was recorded at 30K at an MW frequency of 9.26 GHz, power of 0.06325 mW, modulation frequency of 100 kHz and modulation amplitude 4 G. The copper concentration was estimated to be 50 $\mu$M. The ESR spectra of Cu-AHAHARA complex were acquired in Wilmad tubes using a Bruker Elexsys E500 EPR spectrometer equipped with a cryostat. Peptide stocks at pH 2 were prepared fresh by adding lyophilized solid (>90%) to 10 mM HCl until peptide concentration reached 1 mM. First, Cu(II) solution in water (1 mM, 75 $\mu$L) and peptide stock (1 mM in 10 mM HCl, 150 $\mu$L) were mixed and then buffer (91 mM Hepes, pH 8, 275 $\mu$L) was added to make a solution with 150 $\mu$M Cu(II) and 300 $\mu$M peptide (500 $\mu$L final volume). The mixture was incubated at room temperature for 2 hr, and after glycerol was added to a final concentration of 10%, transferred into an ESR tube and flash frozen in liquid nitrogen. The final pH of the sample was 7.6 as measured by a Spintrode electrode (Hamilton). ESR spectra were acquired at 100 K and 10 K using the following conditions: frequency 9.39 GHz, power 5 mW (D) or 2 mW (C), modulation frequency 100 kHz, modulation amplitude 8 G (10 K) and 4 G (100 K), time constant 163.8 ms. The ESR spectra of CuQu and CuQuA were collected using the Bruker cw ESR EMX spectrometer at the National Biomedical Resource for Advanced ESR Spectroscopy (ACERT). About 100 mg of the air-stable copper complexes were dissolved in 1 mL DMSO. The solutions were poured in 4 mm ESR tubes, frozen in liquid nitrogen and kept in liquid nitrogen Dewar until inserting them in the spectrometer. The spectra were recorded at 100 K, a microwave frequency of 9.316 GHz and attenuation of 30 dB for CuQu and 50 dB for CuQuA.

### *3.3. ESR Spectral Mix*

For multi-component spectral analysis, four mixed spectra were calculated by mixing the ESR spectra of the compounds, CuQu and CuQuA, in proportions of (A) 2:1, (B) 4:1, (C) 10:1 and (D) 20:1 (Figure 9).

## 4. Results and Discussion

### *4.1. Validation of the Analysis*

Interpretation of partially resolved ESR spectra by fitting has been the standard practice in the study of organic radicals and paramagnetic metal complexes. The approximations and the principles of such optimizations remain unknown to the users, whose interpretation of the results is largely dominated by the goodness of the fit and a priori knowledge about the structure or nature of the molecule under investigation. In contrast, a direct extraction of parameters, a process that lacks the visual aids, can raise queries about the accuracy of the outputs. That was our motivation to run the analysis on a series of X-band ESR spectra of Tempol and Tempo under varying oxygen concentration, shown in Figure 3.

Preprints (www.preprints.org) | NOT PEER-REVIEWED | Posted: 21 March 2023 doi:10.20944/preprints202303.0377.v1



The superhyperfine lines are fully or partially resolved in absence of oxygen or when it is present in very low concentration. However, the features become invisible due to line broadening by increased oxygen concentration. Consequently, while the superhyperfine constant in the former cases could be obtained by simple visual inspection or spectral fitting, none of those are applicable in the latter. In all those cases, the WPT-based method recovered the superhyperfine structure from the corresponding ESR spectra and extracted the value of the coupling constant, illustrating both its advantage over the existing spectral analysis approaches and its consistency.

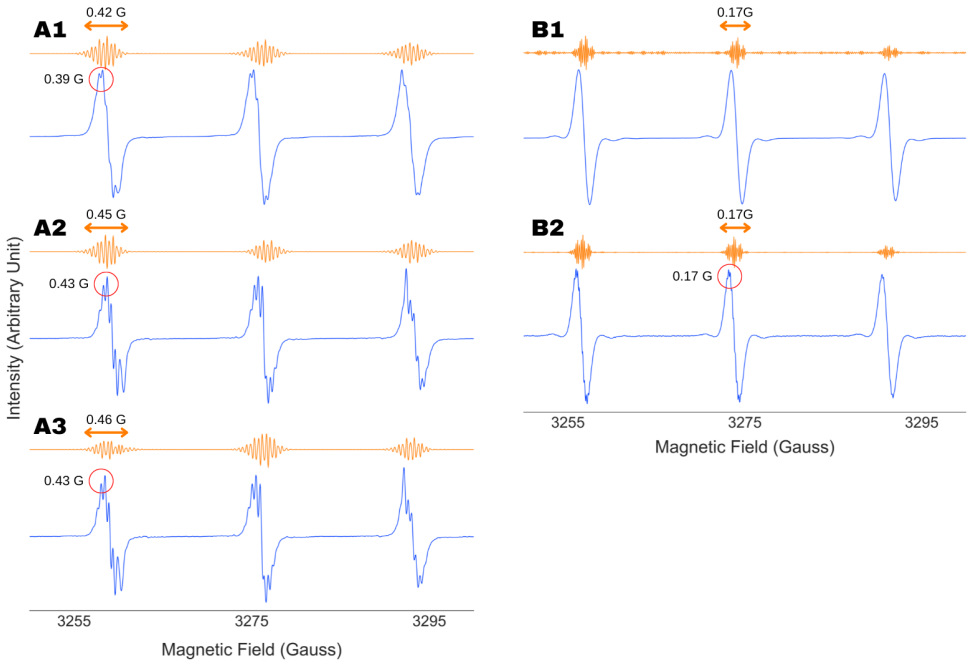


**Figure 3.** Analysis of X-band cw ESR spectra (blue) of Tempol (A) and Tempo (B) under varying concentration of oxygen. The superhyperfine splitting due to the protons are partially resolved in A(1-3) and B2. The superfine splitting is invisible in the fully oxygenated Tempo spectrum (B1) due to line broadening. The superfine spectrum recovered by wavelet packet transform based analysis of the spectra are shown (orange). The similarity between the superfine splitting constant obtained from the WPT analysis and direct analysis of the partially resolved should be noted. The validity of the analysis in case of unresolved spectrum is demonstrated for B1 and B2.

### *4.2. Robustness Against Wavelet Selection*

An important and non-trivial variable in the WPT analysis of ESR spectra is the selection of wavelet or in other words, understanding the robustness of the analysis against the types of wavelets used in the analysis. We repeated the analysis shown in Figure 3 with three different types of wavelets; Coiflet-3 (Coif3), Daubechies-6 (Db6) and Daubechies-9 (Db9), and the results are summarized in Figure 4. The extracted superhyperfine constant values for Tempol and Tempo, $0.44 \pm 0.01$G and $0.20 \pm 0.01$G, showed insignificant variation for all three wavelets, while producing the same number of splitting across all the analysis consistent with the molecular structure. This observation illustrated the robustness of the method, while further validating the accuracy of the extracted parameters. For the rest of the analysis in this work, we used Db9 wavelet.

Preprints (www.preprints.org) | NOT PEER-REVIEWED | Posted: 21 March 2023 doi:10.20944/preprints202303.0377.v1



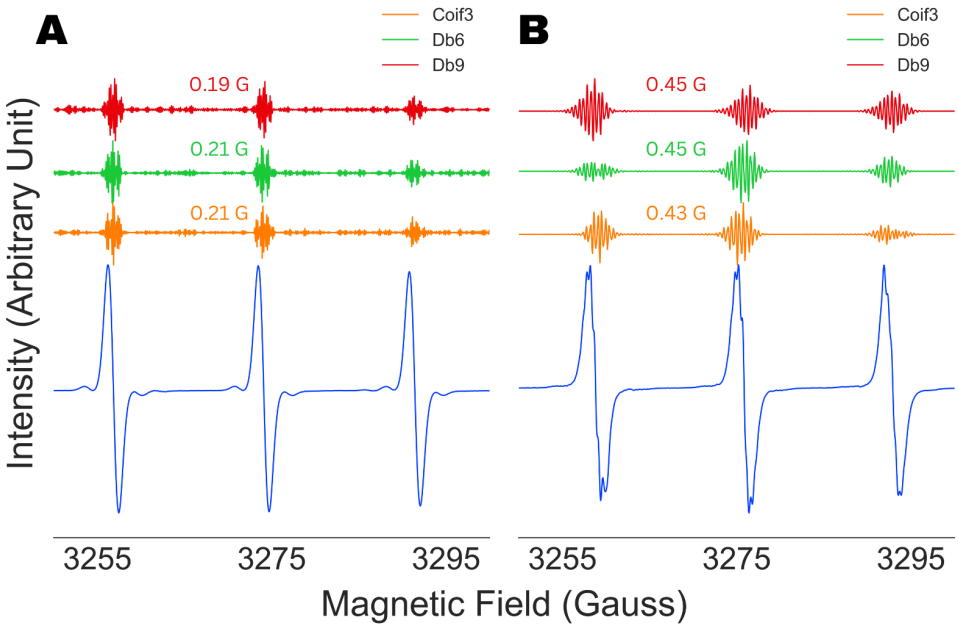


**Figure 4.** Analysis of unresolved and partially resolved X-band cw ESR spectra (blue) of Tempo (A) and Tempol (B). The superfine spectra recovered by wavelet packet transform based analysis of the spectra are shown using three different wavelets, Coiflet-3 (orange), Daubechies-6 (green) and Daubechies-9 (red). Superfine coupling constants obtained are consistent across the analysis involving three different wavelets.

### *4.3. Spectral Analysis of Partially Resolved ESR Spectra*

We started our analysis by fitting the X-band cw ESR spectra of SOD1:H48Q recorded at 30K and Cu-AHAHARA, recorded at 10K and 100K by using the EasySpin software. The optimized simulations along with the experimental spectra are shown in Figure 5. For SOD1:H48Q, the EasySpin analysis yielded nitrogen-hyperfine constant values of 15.6 G (axial) and 9.0 G (parallel), while the simulations for Cu-AHAHARA spectra did not require any nitrogen-hyperfine parameter in fitting the spectra. It should be noted that the Cu-AHAHARA spectrum at 10K shows no nitrogen-hyperfine splitting; however, partial nitrogen-hyperfine splitting is evident for the spectrum at 100K. This apparent anomaly might have resulted from the partial saturation and passage effect [35,36] in case of the former, as evidenced by the behavior of the first integral of the spectrum, and consequently, the EasySpin fit for the 10K spectrum performed poorly compared to that of the 100K spectrum. In addition, the simulation presented for SOD1:H48Q in Figure 5 [A] emphasized the potential presence of a second component, with a slightly shifted $g_{\|}$ and/or different hyperfine coupling constants.

Preprints (www.preprints.org) | NOT PEER-REVIEWED | Posted: 21 March 2023 doi:10.20944/preprints202303.0377.v1



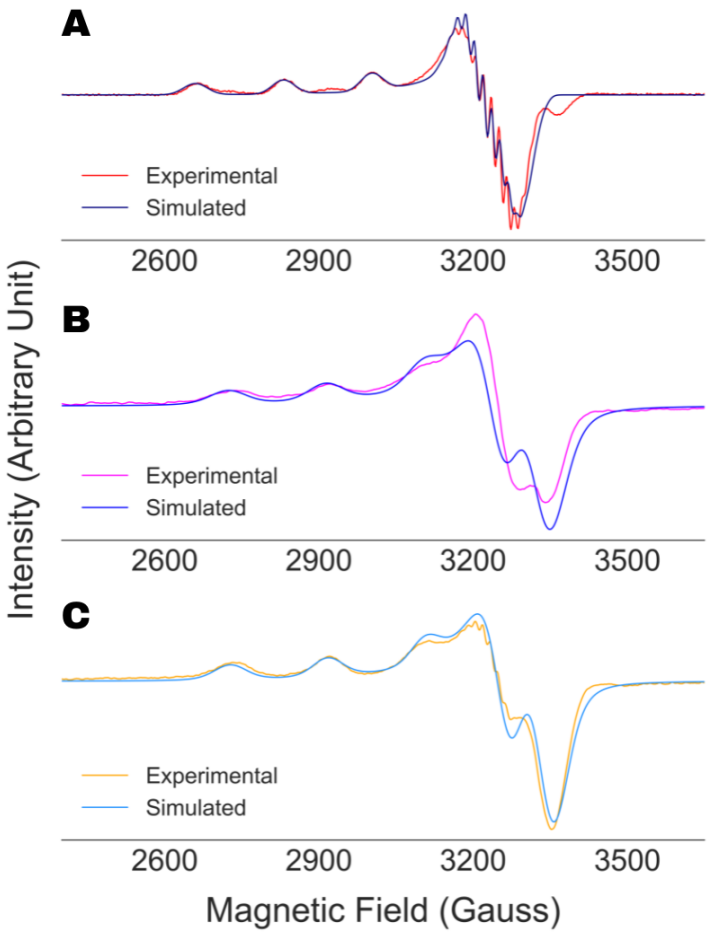


**Figure 5.** EasySpin simulation results along with experimental ESR spectra of SOD1:H48Q (A), Cu-AHAHARA spectrum recorded at 10K (B) and 100K (C).

In Figure 6, we presented the WPT analysis of the ESR spectra of (A) SOD1:H48Q, (B) Cu-AHAHARA at 10K and (C) Cu-AHAHARA at 100K. For all the analysis, the spectra were decomposed to level-4 using the DB9 wavelet. For SOD1:H48Q, our analysis yielded a nitrogen-hyperfine coupling constant of 14.1 G for the axial peaks in the range of 3200 to 3320 G. However, an analysis of the $g_{\|}$ splitting (Figure 6 [A.2]) revealed two different nitrogen-hyperfine splitting constants; 12.5 G along the dominant Cu parallel hyperfine splitting and 16.5 G along the minor component. Following that, we analyzed the splitting along the small axial peak between 3220 and 3400 G (not shown), which emphasized the presence of four nitrogens and a nitrogen-hyperfine constant of $A_N$ = 16.5 G. From this analysis, we could infer a spherical electron density distribution in the second component, suggesting a tetrahedral copper complex with a large hyperfine splitting of $\sim$205 G. Similar analysis for Cu-AHAHARA yielded nitrogen-hyperfine coupling constants of 13.9 G (10K) and 14.0 G (100K) along the $g_{\perp}$ signal component. The consistency of the results demonstrate the robustness of the WPT-based spectral analysis against artifacts, over-saturation effect in this case, which is a major advantage over the standard spectral fitting methods.

Preprints (www.preprints.org) | NOT PEER-REVIEWED | Posted: 21 March 2023 doi:10.20944/preprints202303.0377.v1



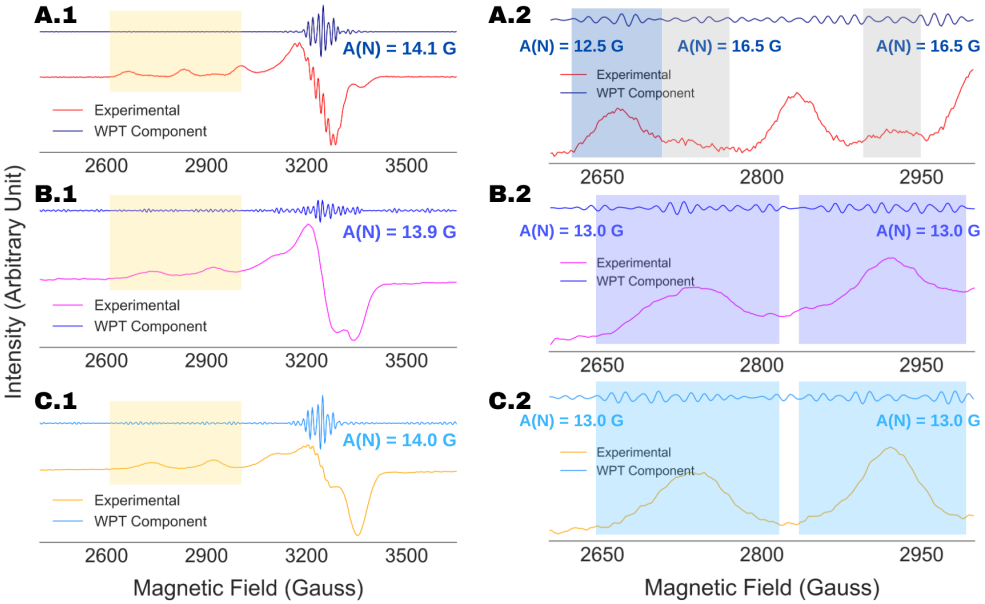


**Figure 6.** Recovery of nitrogen-hyperfine features by WPT analysis from experimental cw ESR spectra of SOD1:H48Q (A), Cu-AHAHARA at 10K (B) and Cu-AHAHARA at 100K (C). The left panel illustrates analysis of the $g_{\perp}$ component, while the $g_{\parallel}$ component is highlighted in yellow and the corresponding analysis is shown on the right. For SOD1:H48Q (A), resolving the nitrogen-hyperfine splitting along $g_{\parallel}$, a dominating component with $A_N$ = 12.5 G (shaded blue) and a minor component with $A_N$ = 16.5 G (shaded gray) were obtained.

It should be noted that the copper coordination geometry of the Cu-AHAHARA complex could not be confirmed in a previous work from the ESR spectral analysis [33]. The WPT analysis presented in Figure 6 suggests strong overlap of nitrogen-hyperfine components in the $g_{\perp}$ region of the ESR spectra at 10K and 100K, while the former seems to contain spectral artifacts, making analysis by standard procedure error-prone. Hence, we analyzed the WPT components originated from the $g_{\parallel}$ region for the both the cases, which is summarized in Figure 7. In case of the spectrum collected at 10K, the WPT component originating from the ESR peak centered 2730 G showed nine evenly spaced lines at 12.5 G apart from each other, indicating an $N_4$-coordination for the copper center in the Cu-AHAHARA complex. In addition, a smaller coupling constant in the $g_{\parallel}$ region in comparison to the value obtained in the $g_{\perp}$ region (13.9 G) suggests four equivalent nitrogens in an axial geometry. This interpretation aligns well with a series of independent experimental and theoretical studies conducted to elucidate the geometry of the complex previously [33]. For the spectrum recorded at 100K, a similar analysis in the $g_{\parallel}$ region did not reproduce the exact same results because of unresolved spectral overlapping in the WPT component. However, upon close inspection, we resolved half of the nitrogen-hyperfine splitting window for the $g_{\parallel}$ peaks centered at 2734 G and 2901 G. In this regard, it should be noted that only the even spacing between the peaks in a WPT component around a $g_{\parallel}$ peak was used as the criteria for recovering nitrogen-hyperfine splitting. The WPT analysis is highly accurate in recovering spectral information with respect to their location, but not necessarily the intensity. Factors like partial overlapping of resonance lines, residual noise and spectral artifacts affects the intensities of the peaks in a WPT component and hence, the recovered superfine splitting is unlikely to reproduce the relative intensity pattern expected for perfectly resolved spectra. The analysis of the Cu-AHAHARA ESR spectrum at 100K yielded the same nitrogen-hyperfine coupling constant of 12.5 G and suggested an $N_4$ coordination for the copper center.

 doi:10.20944/preprints202303.0377.v1



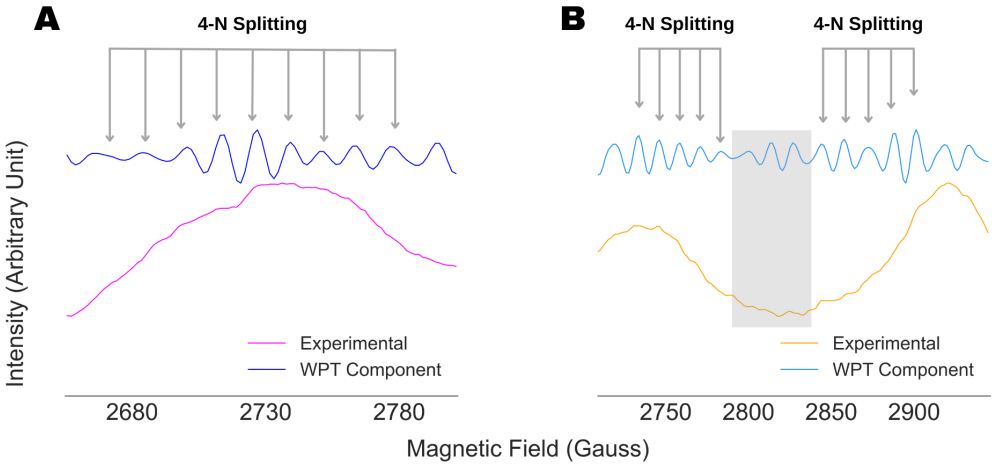


**Figure 7.** Analysis of the $g_{\parallel}$ components in the ESR spectra of Cu-AHAHARA complex at (A) 10K and (B) 100K for probing the copper coordination. For (A), the splitting pattern observed in the WPT component between 2650 G and 2800 G revealed nine equally spaced lines centered at 2727 G with inter-peak spacing of 12.5 G, indicating four nitrogens in the copper coordination sphere. In case of (B), the entire range of nitrogen-hyperfine splitting for none of the $g_{\parallel}$ components were visible due to overlapping in the WPT component. However, for both the $g_{\parallel}$ components centered at 2734 G and 2901 G, half of the nitrogen-hyperfine splitting windows were resolved, indicating four nitrogen coordination geometry for the copper center with a coupling constant of 12.5 G. The WPT component in the shaded region (gray) was not considered in the analysis because of varying inter-peak spacing in the region.

The WPT analysis for the X-band ESR spectra of two copper-nitrogen complexes, CuQu and CuQuA, are shown in Figure 8. The detail component in the optimal level of decomposition, which was 3 for both the spectra, revealed unresolved hyperfine structure due to nitrogens coordinated to the copper centers in the complexes. For example, Cu(II) splits the resonance line at $g_{\perp}$ into four lines, we will call them h-1, h-2, h-3 and h-4 for explanation purpose. Each of these lines split further due to the $n$ interacting nitrogens into $m = (2 \times n + 1)$ lines. Given the small magnetic field window between h-1 and h-4, as well as the nitrogen-hyperfine coupling, most of the resonance lines cannot be resolved due to complete or partial overlapping. However, for most of the cases, it might be possible to identify the first $m/2$ lines originating from h-1 and the last $(m+1)/2$ lines originating from h-4, where the extent of overlapping of resonance lines is the least. Using this logic, from the detail component analysis for CuQu in Figure 8**A**, we identified 3 lines with a total separation of 53 G, which corresponded to an $m = 5$ or 2 coupled nitrogens with h-1 and h-4 at 3203 G and 3314 G. Further, we calculated the nitrogen-hyperfine coupling constant to be $A(\mathrm{N}) = 53/2$ G or 26.5 G, the Cu(II) hyperfine coupling $A(\mathrm{Cu}) = (3314 - 3203)/3$ G or 37 G and the $g_{\perp} = (3314 + 3203)/2$ G $\equiv 2.0427$. The calculated spin-Hamiltonian parameters are in good agreement with previously reported analogous $N_2O_2$-coordinated copper(II) complexes [37,38]. With a similar analysis for CuQuA, Figure 8**B**, we inferred that 3 nitrogens were coordinating with the Cu(II) center with $A(\mathrm{N}) = 21.3$ G, while the $g_{\perp}$ and $A(\mathrm{Cu})$ were calculated to be 2.0411 and 23.3 G. The original $N_2O_2$ coordination geometry for the copper center observed in CuQu complex can be expanded in CuQuA due to the presence of peripheral amine in the QuA ligand scaffold. The potential involvement of one amine group is supported by the EPR data, indicating an $N_3O_2$ coordination.

Preprints (www.preprints.org) | NOT PEER-REVIEWED | Posted: 21 March 2023 doi:10.20944/preprints202303.0377.v1



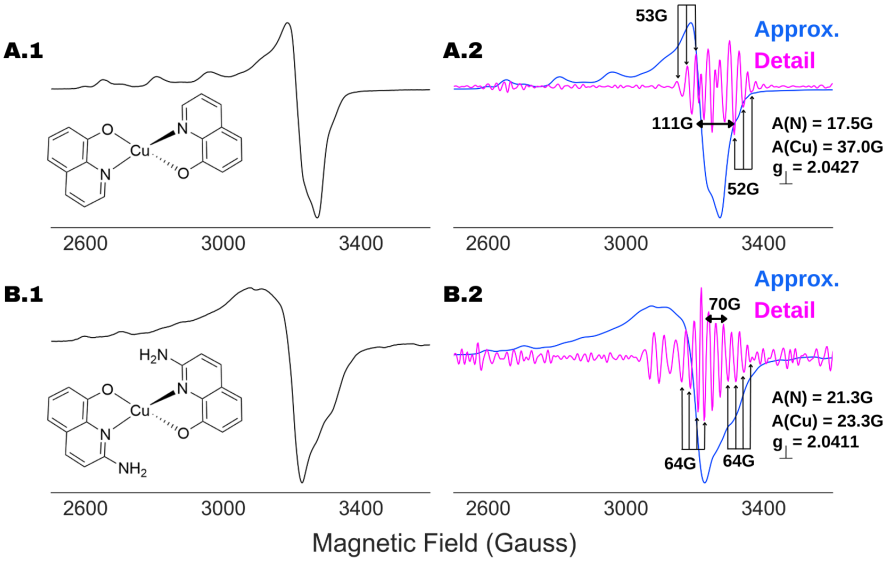


**Figure 8.** Recovery of nitrogen-hyperfine structure and coordination of Cu(II) center in (A) CuQu and (B) CuQuA. Both the ESR spectra (left panel) were recorded at 100K and an ESR frequency of 9.316 GHz with attenuation of (A) 30 db and (B) 50 db, respectively. The approximation (blue) and detail (magenta) spectral components originated at the optimal decomposition level of 3 are shown in the right panel (scaled arbitrarily for visualization purpose). For both the cases, the nitrogen superfine structure were identified, showing (A) 2-N and (B) 3-N coordination to the copper centers in the two cases, along with the position of $g_\perp$ and hyperfine coupling due to Cu(II).

### *4.4. Analysis of Multi-Component ESR Spectra*

It has already been shown in Figure 6 that the spectral analysis of the $g_\parallel$ components in the ESR spectrum of SOD1:H48Q revealed the presence of two components. In this section, we present further proof of how the WPT-based spectral analysis can be utilized efficiently in identifying multi-component spectra, even when the components are present in highly disproportionate amounts. A set of four mixed spectra was produced for the analysis by mixing the ESR spectra of CuQu and CuQuA in proportions of (A) 2:1, (B) 4:1, (C) 10:1 and (D) 20:1, shown in Figure 9. The WPT spectral analysis was conducted using Db9 wavelet at decomposition level of 4 and the WPT detail components for the spectral region between 2600 and 2775 G are shown in the insets of Figure 9. In all the cases, 5 lines with a splitting constant of 17 G were recovered between 2610 and 2670 G, which corresponds to CuQu, which is expected because of the abundance of the complex in the mixtures. However, a second component with a splitting constant of 16 G was identified in between 2700 and 2748 G. For the latter, only 4 or 3 lines were visible due to spectral overlap, but it can be separated from artifacts by the consistent positions of the peaks appearing the detail WPT component. It should be noted that this strategy clearly identifies a second minor component directly from the spectral analysis, in this case CuQuA, but it may not be possible to determine the structure of the component solely from the analysis due to spectral overlaps, leading to unrecoverable information loss. However, we like to emphasize that we used poorly resolved X-band ESR spectra of the individual complexes and given such constraints, we believe that it is a major achievement to detect a second component solely from ESR spectral analysis, even when the second component is present at as low a relative concentration as of 5%. In general, such findings from the WPT spectral analysis will help researchers decide on further structural analysis by employing high-frequency ESR and/or complementary techniques.

Preprints (www.preprints.org) | NOT PEER-REVIEWED | Posted: 21 March 2023 doi:10.20944/preprints202303.0377.v1



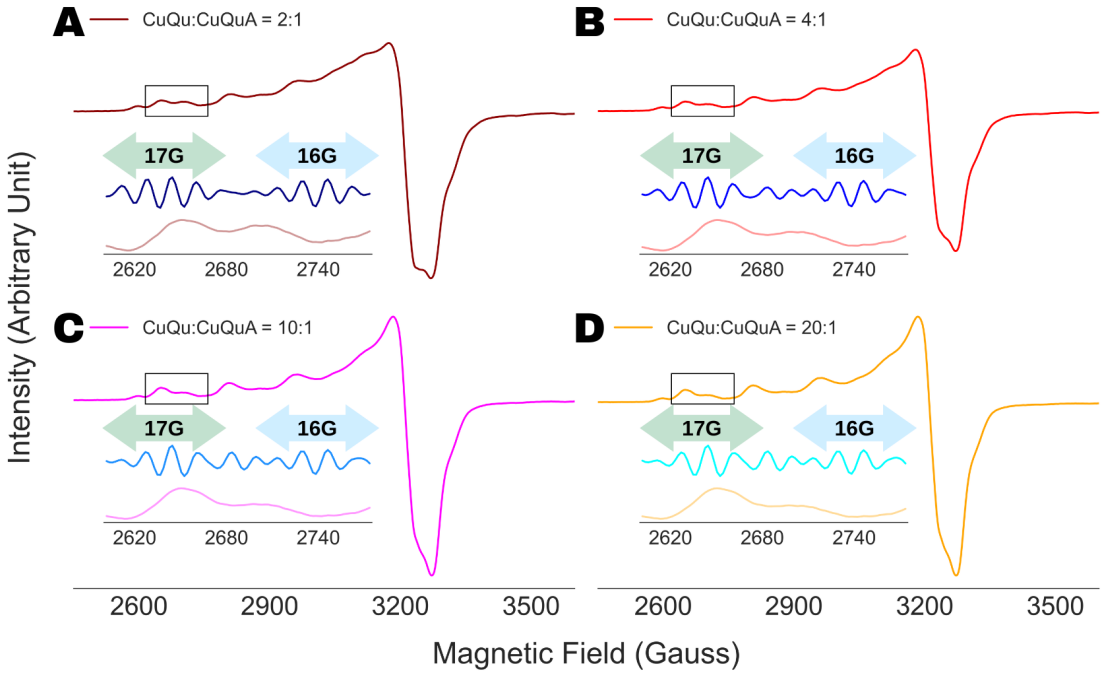


**Figure 9.** WPT analysis of ESR spectra of mixtures of CuQu and CuQuA, mixed in proportions of (A) 2:1, (B) 4:1, (C) 10:1 and (D) 20:1, respectively. The insets show the WPT component for the spectral region between 2600 G and 2775 G. Two components were identified in each of the spectral analysis from the difference in nitrogen-hyperfine splitting of 17 G (green double headed arrow) and 16 G (blue double headed arrow).

## 5. Conclusions

In this work, we have provided the complete recipe for a simulation-free analysis of cw ESR spectra using a wavelet packet transform-based algorithm and experimental X-band ESR spectra of organic free radicals (Tempol and Tempo) and metal complexes (copper (II) inorganic and biological complexes). We showcased three major accomplishments of the WPT-based spectral analysis over standard simulations: (1) direct extraction of nitrogen-hyperfine structure from poorly resolved / unresolved spectra, (2) insensitivity toward spectral artifacts and (3) identification of multi-component samples. Consistent extraction of superhyperfine coupling constant due to protons from both partially resolved and unresolved spectra for Tempol is presented, validating the accuracy of the new spectral analysis technique. The limitations of standard ESR spectral analysis are illustrated by running EasySpin simulations for partially resolved and poorly resolved spectra, with one of the cases containing some experimental artifacts. While the accuracy and efficiency of the simulations varied drastically in those cases, the WPT-based analysis extracted spectral parameters, revealing hyperfine and superhyperfine splittings not detectable by EasySpin, and the analysis was unperturbed by spectral artifacts. For the copper-nitrogen complexes, the resolved hyperfine structures confirmed the number of nitrogen atoms coordinating with copper centers as well as their coordination geometry. Finally, by close examination of the detail WPT components originating from the $g_{||}$-regions of the spectra, the presence of two different components in case of SOD1:H48Q, a mutant of SOD1, has been confirmed along with their nitrogen-hyperfine coupling constants. The strength of the method in resolving multi-component spectra has been displayed further by analyzing four mixed spectra of two copper-nitrogen complexes, CuQu and CuQuA. The spectral analysis revealed the presence of the two components even when the proportion of the two components in the spectrum was 20:1. In addition, three different wavelets were used for selected cases, emphasizing the robustness of the method against the choice of wavelets. The comprehensive analysis presented in this work is expected to motivate broad adoption

 doi:10.20944/preprints202303.0377.v1



of the technique in analysing ESR spectra and the spectral parameters obtained from the analysis can be further optimized using simulations and/or other computational methods.

**Author Contributions:** Conceptualization, A.S.R., B.D., and M.S.; methodology, A.S.R., B.D., and M.S.; formal analysis, A.S.R., and B.D.; material synthesis, A.D., B.D., D.D., and O.M.; spectral data collection, A.S.R., B.D., and O.M.; investigation, A.S.R.; writing—original draft preparation, A.S.R.; writing—review and editing, O.M., A.D., and M.S.; visualization, A.S.R.; supervision, M.S.; project administration, M.S.; funding acquisition, M.S. and A.D. All authors have read and agreed to the published version of the manuscript.

**Funding:** Data were collected at the ACERT facility for ESR on Cornell's campus (the National Institute of General Medical Sciences/National Institutes of Health under grant R24GM146107). This research was funded in part by the DST-SERB ore research grant (CRG/2020/001239).

**Data Availability Statement:** The data used in this paper can be accessed via https://github.com/Signal-Science-Lab/Simulation_Independent_ESR_Spectral_Analysis.

**Conflicts of Interest:** The authors declare no conflict of interest.

## Abbreviations

The following abbreviations are used in this manuscript:

| | |
|---|---|
| ESR | Electron spin resonance |
| WPT | Wavelet packet transform |
| NERD | Noise Elimination and Reduction via Denoising |
| SOD1 | Superoxide dismutase-1 |


1. Mabbs, F.E.; Collison, D. *Electron paramagnetic resonance of d transition metal compounds*; Elsevier, 2013.
2. Fukuzumi, S.; Ohkubo, K. Quantitative evaluation of Lewis acidity of metal ions derived from the g values of ESR spectra of superoxide: Metal ion complexes in relation to the promoting effects in electron transfer reactions. *Chemistry–A European Journal* **2000**, *6*, 4532–4535.
3. Matsuda, K.; Takayama, K.; Irie, M. Photochromism of metal complexes composed of diarylethene ligands and Zn (II), Mn (II), and Cu (II) hexafluoroacetylacetonates. *Inorganic Chemistry* **2004**, *43*, 482–489.
4. Raman, N.; Dhaveethu Raja, J.; Sakthivel, A. Synthesis, spectral characterization of Schiff base transition metal complexes: DNA cleavage and antimicrobial activity studies. *Journal of Chemical Sciences* **2007**, *119*, 303–310.
5. Lund, A.; Shiotani, M.; Shimada, S. *Principles and applications of ESR spectroscopy*; Springer Science & Business Media, 2011.
6. Kohno, M. Applications of electron spin resonance spectrometry for reactive oxygen species and reactive nitrogen species research. *Journal of Clinical Biochemistry and Nutrition* **2010**, pp. 1006170036–1006170036.
7. Khramtsov, V.V.; Volodarsky, L.B. Use of imidazoline nitroxides in studies of chemical reactions ESR measurements of the concentration and reactivity of protons, thiols, and nitric oxide. In *Biological Magnetic Resonance*; Springer, 2002; pp. 109–180.
8. Lazreg, F.; Nahra, F.; Cazin, C.S. Copper–NHC complexes in catalysis. *Coordination Chemistry Reviews* **2015**, *293*, 48–79.
9. Ali, A.; Prakash, D.; Majumder, P.; Ghosh, S.; Dutta, A. Flexible Ligand in a Molecular Cu Electrocatalyst Unfurls Bidirectional O2/H2O Conversion in Water. *ACS Catalysis* **2021**, *11*, 5934–5941.
10. Chen, Z.; Meyer, T.J. Copper (II) catalysis of water oxidation. *Angewandte Chemie International Edition* **2013**, *52*, 700–703.
11. Weng, Z.; Wu, Y.; Wang, M.; Jiang, J.; Yang, K.; Huo, S.; Wang, X.F.; Ma, Q.; Brudvig, G.W.; Batista, V.S.; et al. Active sites of copper-complex catalytic materials for electrochemical carbon dioxide reduction. *Nature Communications* **2018**, *9*, 1–9.
12. Bolm, C.; Martin, M.; Gescheidt, G.; Palivan, C.; Neshchadin, D.; Bertagnolli, H.; Feth, M.; Schweiger, A.; Mitrikas, G.; Harmer, J. Spectroscopic investigations of bis (sulfoximine) copper (II) complexes and their relevance in asymmetric catalysis. *Journal of the American Chemical Society* **2003**, *125*, 6222–6227.
13. Bonke, S.A.; Risse, T.; Schnegg, A.; Brückner, A. In situ electron paramagnetic resonance spectroscopy for catalysis. *Nature Reviews Methods Primers* **2021**, *1*, 33.
14. Sánchez-Moreno, C. Methods used to evaluate the free radical scavenging activity in foods and biological systems. *Food Science and Technology International* **2002**, *8*, 121–137.
15. Okano, H. Effects of static magnetic fields in biology: Role of free radicals. *Frontiers in Bioscience-Landmark* **2008**, *13*, 6106–6125.
16. Yin, H.; Xu, L.; Porter, N.A. Free radical lipid peroxidation: Mechanisms and analysis. *Chemical Reviews* **2011**, *111*, 5944–5972.
17. Eaton, G.R.; Eaton, S.S.; Barr, D.P.; Weber, R.T. *Quantitative EPR*; Springer Science & Business Media, 2010.
18. Murphy, D.M.; Farley, R.D. Principles and applications of ENDOR spectroscopy for structure determination in solution and disordered matrices. *Chemical Society Reviews* **2006**, *35*, 249–268.

 doi:10.20944/preprints202303.0377.v1




19. Golombek, A.P.; Hendrich, M.P. Quantitative analysis of dinuclear manganese (II) EPR spectra. *Journal of Magnetic Resonance* **2003**, *165*, 33–48.
20. Drew, S.C.; Young, C.G.; Hanson, G.R. A density functional study of the electronic structure and spin hamiltonian parameters of mononuclear thiomolybdenyl complexes. *Inorganic Chemistry* **2007**, *46*, 2388–2397.
21. Cox, N.; Jin, L.; Jaszewski, A.; Smith, P.J.; Krausz, E.; Rutherford, A.W.; Pace, R. The semiquinone-iron complex of photosystem II: Structural insights from ESR and theoretical simulation; evidence that the native ligand to the non-heme iron is carbonate. *Biophysical Journal* **2009**, *97*, 2024–2033.
22. Trukhan, S.N.; Yakushkin, S.S.; Martyanov, O.N. Fine-tuning simulation of the ESR spectrum– Sensitive tool to identify the local environment of asphaltenes in situ. *The Journal of Physical Chemistry C* **2022**.
23. Stoll, S.; Schweiger, A. EasySpin, a comprehensive software package for spectral simulation and analysis in EPR. *Journal of Magnetic Resonance* **2006**, *178*, 42–55.
24. Khairy, K.; Budil, D.; Fajer, P. Nonlinear-least-squares analysis of slow motional regime EPR spectra. *Journal of Magnetic Resonance* **2006**, *183*, 152–159.
25. Srivastava, M.; Dzikovski, B.; Freed, J.H. Extraction of Weak Spectroscopic Signals with High Fidelity: Examples from ESR. *The Journal of Physical Chemistry A* **2021**, *125*, 4480–4487.
26. Roy, A.S.; Srivastava, M. Hyperfine Decoupling of ESR Spectra Using Wavelet Transform. *Magnetochemistry* **2022**, *8*, 32.
27. Sinha Roy, A.; Srivastava, M. Analysis of Small-Molecule Mixtures by Super-Resolved 1H NMR Spectroscopy. *The Journal of Physical Chemistry A* **2022**, *126*, 9108–9113.
28. Sinha Roy, A.; Srivastava, M. Unsupervised Analysis of Small Molecule Mixtures by Wavelet-Based Super-Resolved NMR. *Molecules* **2023**, *28*, 792.
29. Srivastava, M.; Anderson, C.L.; Freed, J.H. A New Wavelet Denoising Method for Selecting Decomposition Levels and Noise Thresholds. *IEEE Access* **2016**, *4*, 3862–3877.
30. Addison, P. *The Illustrated Wavelet Transform Handbook: Introductory Theory and Applications in Science, Engineering, Medicine and Finance*, 2 ed.; CRC Press: London, UK, 2016.
31. Wang, Q.; Johnson, J.L.; Agar, N.Y.; Agar, J.N. Protein aggregation and protein instability govern familial amyotrophic lateral sclerosis patient survival. *PLoS Biology* **2008**, *6*, e170.
32. Pratt, A.J.; Shin, D.S.; Merz, G.E.; Rambo, R.P.; Lancaster, W.A.; Dyer, K.N.; Borbat, P.P.; Poole, F.L.; Adams, M.W.; Freed, J.H.; et al. Aggregation propensities of superoxide dismutase G93 hotspot mutants mirror ALS clinical phenotypes. *Proceedings of the National Academy of Sciences* **2014**, *111*, E4568–E4576.
33. Makhlynets, O.V.; Gosavi, P.M.; Korendovych, I.V. Short Self-Assembling Peptides Are Able to Bind to Copper and Activate Oxygen. *Angewandte Chemie International Edition* **2016**, *55*, 9017–9020.
34. Merz, G.E.; Borbat, P.P.; Pratt, A.J.; Getzoff, E.D.; Freed, J.H.; Crane, B.R. Copper-based pulsed dipolar ESR spectroscopy as a probe of protein conformation linked to disease states. *Biophysical Journal* **2014**, *107*, 1669–1674.
35. Ernst, R.; Anderson, W. Sensitivity enhancement in magnetic resonance. II. Investigation of intermediate passage conditions. *Review of Scientific Instruments* **1965**, *36*, 1696–1706.
36. Portis, A. Rapid passage effects in electron spin resonance. *Physical Review* **1955**, *100*, 1219.
37. Noël, S.; Perez, F.; Pedersen, J.T.; Alies, B.; Ladeira, S.; Sayen, S.; Guillon, E.; Gras, E.; Hureau, C. A new water-soluble Cu (II) chelator that retrieves Cu from Cu (amyloid-$\beta$) species, stops associated ROS production and prevents Cu (II)-induced A$\beta$ aggregation. *Journal of Inorganic Biochemistry* **2012**, *117*, 322–325.
38. Bunda, S.; May, N.V.; Bonczidai-Kelemen, D.; Udvardy, A.; Ching, H.V.; Nys, K.; Samanipour, M.; Van Doorslaer, S.; Joo, F.; Lihi, N. Copper (II) complexes of sulfonated salan ligands: Thermodynamic and spectroscopic features and applications for catalysis of the Henry reaction. *Inorganic Chemistry* **2021**, *60*, 11259–11272.